NMR Structure of a *de Novo* Designed, Peptide 33mer with Two Distinct, Compact β-Sheet Folds†

Elena Ilyina, Vikram Roongta, and Kevin H. Mayo*

Department of Biochemistry, Biomedical Engineering Center, University of Minnesota Health Sciences Center, 420 Delaware Street, S.E., Minneapolis, Minnesota 55455

Received December 13, 1996; Revised Manuscript Received February 11, 1997[⊗]

ABSTRACT: A *de novo* designed 33-residue polypeptide folds as a compact β-sheet sandwich tetramer in aqueous solution. NMR structural analysis shows that although monomer subunits have the same three-stranded antiparallel β-sheet fold, two equally populated conformational states are identified. Conformational heterogeneity arises from formation of two distinct dimer folds. Each dimer is formed by continuing the monomer β-sheet into a six-stranded sheet similar to that found in α-chemokines. Dimer heterogeneity arises primarily from a two-residue shift in the alignment of interfacial strands. NOE-based conformational modeling has yielded well-defined structures for both dimer types. While the tetramer β-sheet sandwich most probably results from association of hydrophobic surfaces from two amphipathic dimers, dimers could combine to form either two types of homotetramers and/or one heterotetramer composed of both dimer types. Even though interdimer NOEs could not be unambiguously identified to resolve this point, thermodynamic arguments based on observation of equal populations of both dimer types favor formation of heterotetramers.

De novo design of peptides has helped in understanding the principles behind protein folding and in designing proteins with new and improved functions (e.g., Regan & DeGrado, 1988; DeGrado et al., 1989; Hecht et al., 1990; Hahn et al., 1990; Fedorov et al., 1992; Richardson et al., 1992; Handel et al., 1993; Kamteker et al., 1993; Quinn et al., 1994; Fezoui, et al., 1994; Kuroda et al., 1994; Bryson et al., 1995). Designing α-helix, helix bundle, coiled-coil, and β-turn peptides has dominated the field. Designing β-sheet peptides has proven more complicated due to their limited solubility via aggregation in water and due to the nature of their folding which is dictated by long range interactions. Recently, this was circumvented in a water-soluble designed α/β peptide (Struthers et al., 1996) which folds as a compact monomer with an amphipathic α-helix stacked on to a two-stranded amphipathic β-sheet. However, up to now designing a compact, purely β-sheet-containing peptide has met with limited success. The betabellin series (Richardson et al., 1992) and betadoublet (Quinn et al., 1994) peptides, for example, show limited solubility in water (and primarily at lower pH values) and noncompact β-sheet conformational properties, as monitored by CD and NMR.[1] Betabellin 14D (Yan & Erickson, 1994) is the best in that series and yet does not give a good compact fold even with a covalent disulfide bond between two sandwiched monomers.

β-Sheet peptide designs usually have been based on one of a number of structural propensity scales (e.g., Kim & Berg, 1993; Minor & Kim, 1994a,b; Smith et al., 1994) which are derived either statistically from structural databases of known folded proteins or by making single or minimal site-specific changes in a fully folded protein. Although use of such scales has helped in designing, for example, a short β-hairpin peptide (Blanco et al., 1994; Searle et al., 1995) which remains monomeric in water, larger *de novo* designed β-sheet-forming peptides like betadoublet and betabellin have been inherently designed to self-associate through their otherwise solvent-exposed amphipathic hydrophobic surface. Their limited solubility in water and their inability to form compact β-sheet structure may indicate that such scales are generally less useful (Otzen & Fersht, 1995) when designing larger β-sheet-forming amphipaths.

Recently, peptide 33mers derived from the β-sheet domains of α-chemokine proteins (Miller & Krangel, 1992) platelet factor 4 (PF4) (Ilyina & Mayo, 1995) and interleukin 8 (IL-8) (Mayo et al., 1996) have been shown to form self-association-induced β-sheet structure like that in their native protein counterparts. The folding and solubility properties of these α-chemokine peptides as well as those of betabellins and betadoublet have been exploited in the design of novel water-soluble, self-association-induced β-sheet-forming peptides (Mayo et al., 1996). The intricate interplay among precipitation, solvation, and folding was overcome by maximizing those combinations of amino acid residues in a sequence which promote β-sheet sandwich folding under physiologic conditions. One peptide, βpep-4, designed by using this approach, was found to fold compactly as a β-sheet-containing peptide tetramer (Mayo et al., 1996). Here, we report the NMR solution structure of βpep-4.

† This work was supported by generous research grants from the Minnesota Medical Foundation and the Graduate School of the University of Minnesota.

* Address correspondence to this author.

⊗ Abstract published in *Advance ACS Abstracts,* April 1, 1997.

[1] Abbreviations: NMR, nuclear magnetic resonance; 2D-NMR, two-dimensional NMR spectroscopy; DQF-COSY, 2D-NMR double-quantum-filtered correlated spectroscopy; TOCSY, 2D-NMR homonuclear Hartman−Hahn total correlated spectroscopy; NOE, nuclear Overhauser effect; NOESY, 2D-NMR nuclear Overhauser effect spectroscopy; rf, radio frequency; FID, free induction decay; RMSD, root mean squared deviation; PF4, platelet factor 4; IL-8, interleukin 8; Gro-α, growth-related protein α.

S0006-2960(96)03064-4 CCC: $14.00

MATERIALS AND METHODS

Peptide Synthesis. The 33-residue peptide βpep-4 has the amino acid sequence: SIQDLNVSMKLFRKQAKWKI-IVKLNDGRELSLD. The peptide was synthesized on a Milligen Biosearch 9600 peptide synthesizer using procedures based on Merrifield solid-phase synthesis with Fmoc-BOP chemistry (Stewart & Young, 1984). After the sequence had been obtained, the peptide support and side chain protection groups were acid (trifluoroacetic acid and scavanger mixture) cleaved. The C-terminal aspartic acid residue Cα carboxylate was made in the amide form. Crude peptide was anaylzed for purity on a Hewlett-Packard 1090M analytical HPLC using a reverse-phase C18 VyDac column. Peptide generally was about 90% pure. Further purification was done on a preparative reverse-phase HPLC C-18 column using an elution gradient of 0−60% acetonitrile with 0.1% trifluoroacetic acid in water. Peptide then was analyzed for amino acid composition on a Beckman 6300 amino acid analyzer by total hydrolysis of samples using 6 N HCl at 110 °C for 18−20 h. N- Terminal sequencing confirmed peptide purity.

NMR Measurements. For NMR measurements, freeze-dried peptide was dissolved either in D_2O or in H_2O/D_2O (9:1). Protein concentration normally was in the range of 1−5 mM. pH was adjusted by adding microliter quantities of NaOD or DCl to the peptide sample. NMR spectra were acquired on a Bruker AMX-600 or AMX-500 NMR spectrometer.

For resonance assignments, double-quantum-filtered COSY (Piantini et al., 1982; Shaka & Freeman, 1983) and 2D-homonuclear magnetization transfer (TOCSY) spectra, obtained by spin-locking with a MLEV-17 sequence (Bax & Davis, 1985) with a mixing time of 60 ms, were used to identify spin systems. NOESY experiments (Jeener et al., 1979; Wider et al., 1984) were performed to sequentially connect spin systems and to identify NOE connectivities. All 2D-NMR spectra were acquired in the TPPI (Marion & Wüthrich, 1983) or States-TPPI (States et al., 1982; Marion et al., 1989) phase-sensitive mode. The water resonance was suppressed by direct irradiation (0.8 s) at the water frequency during the relaxation delay between scans as well as during the mixing time in NOESY experiments.

2D-NMR spectra were collected as 256−400 $t1$ experiments, each with 1K or 2K complex data points over a spectral width of 6 kHz in both dimensions with the carrier placed on the water resonance. For TOCSY, COSY, and NOESY spectra, normally 16 and 64 scans, respectively, were time averaged per $t1$ experiment. The data were processed directly on the Bruker AMX-600 X-32 or offline on a Bruker Aspect-1 workstation with the Bruker UXNMR program. Data sets were multiplied in both dimensions by a 30−60° shifted sine-bell function and zero-filled to 1K in the $t1$ dimension prior to Fourier transformation.

Conformational Modeling. NMR/NOE-derived internuclear distance constraints were used in calculating structures for βpep-4 by using X-PLOR (Brunger, 1992). Monomeric βpep-4 was created using parallhdg.pro force fields. The monomer was then duplicated into A, B, C, and D subunits for both βpep-4 dimer types. Since each dimer contains one $C2$ symmetry axis, a symmetry table was created and noncrystallographic symmetry (NCS) restraints were applied from backbone positions N6 to R13, W18 to K23, and E29 to L32, but not for the apparently less structured loops and terminal residues. A 0.2 Å variation between monomers was allowed. For NOE constraints, a soft potential function was used. The first step in our X-PLOR protocol created a template coordinate set by using the *Template* routine. Then 100 random structures were generated and refined using the *Random* and *Refine* routines, respectively. This dynamical simulated annealing procedure ran high temperature dynamics (2000 K for 50 ps), and cooled down (to 100 K in 50 K steps with 1.3 ps molecular dynamics at each temperature step) and energy minimized the structures. The distance symmetry force constant was kept at 1.0 kcal·mol^{-1}·Å^{-2} throughout the calculation. The NCS force constant for the first phase of the simulated annealing protocol was kept at 0.1 kcal·mol^{-1}Å^{-2}. The NOE force constant was increased by a factor of 2 at the beginning of each cycle, from an initial value of 2 to a maximum value of 25 kcal·mol^{-1}Å^{-2}, while the van der Waals force constant was increased slowly from 0.01 to 4 kcal·mol^{-1}Å^{-2}. Powell minimization was then performed at 100 K for 250 steps. The resulting structures were subjected to the same *Refine* routine two times. Significant reductions in E_{total} and E_{noe} were noted with each *Refine* cycle. Twenty-five structures were then superimposed using the INSIGHT (Biosym/MSI, San Diego, CA) viewer and analyzed using X-PLOR analysis routines. Final structures were subjected to the X-PLOR *Accept* routine with the violation threshold for NOEs and dihedral angles as shown in Table 2. Structures showed fewer than ten violations for an NOE threshold of 0.5 Å (Nilges, 1993). All computations were performed on Silicon Graphics (SGI) 4 R-4400 Challenge L CPUs and analyzed on SGI Indigo Extreme workstations using the program INSIGHT.

RESULTS AND DISCUSSION

The ^{1}H NMR spectrum of βpep-4 indicates that the peptide 33mer folds relatively compactly (Mayo et al., 1996). If βpep-4 folded in a single conformation, no more than 33 αN cross-peaks would be observed in any COSY-like 2D NMR spectrum. βpep-4, however, shows considerably more than 33 αN cross-peaks, indicating conformational heterogeneity. TOCSY spectral analysis shows the presence of duplicate cross-peaks for the spin systems of many residues. Figure 1A exemplifies this in the downfield αN region from a TOCSY spectrum. Several clearly distinguishable pairs of equally intense cross-peaks, showing the same spin-system signature, are boxed-in. In this respect, NMR data indicate the presence of two major, equally populated conformational states.

Since many resonances in both conformational states were resolved, state-specific sequential assignments could be made by analyzing COSY, TOCSY, and NOESY data. A number of these sequence-specific resonance assignments are labeled in Figure 1, and all known assignments are available as supporting information. Resonances belonging to S1−Q3, K14−K17, and N25−G27 could not be sequentially assigned, and of these only S1, I2, A16, and G27 could be identified by their characteristic spin-system signatures. Spin-system signatures for Q3, Q15, and N25, and D26 could be identified, but these could not be uniquely assigned. State-specific sequential resonance assignments have been made for all other residues, and conformational states are designated as state 1 and state 2.

Initially, the observation of downfield shifted αH and NH resonances strongly suggested β-sheet conformation (Wishart

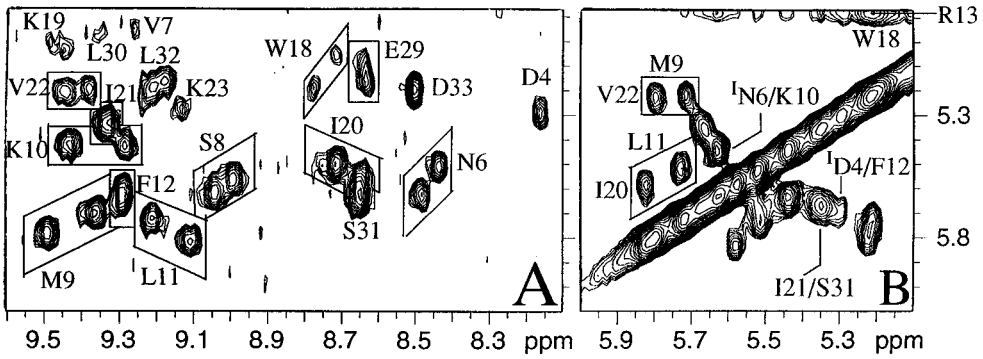

FIGURE 1: TOCSY and NOESY spectra of βpep-4. ^{1}H resonance regions from 2D-NMR TOCSY and NOESY contour plots are shown for βpep-4 peptide (20 mg/mL) in 20 mM potassium phosphate, pH 6.3, 40 °C. Data were collected in $^1H_2O/^2H_2O$ (90:10) (TOCSY, panel A) and in ^2H_2O (99.99%) (NOESY, panel B). 256 hypercomplex FIDs containing 2K words each were collected, zero-filled to 1024 in $t1$, and multiplied by a 60° shifted sine-squared function in $t1$ and $t2$ prior to Fourier transformation. The NOESY mixing time was 0.2 s, and the TOCSY spin-lock time was 60 ms. Labeling of resonances is as discussed in the text. Boxed-in cross-peaks denote duplicate resonances, one from each conformational state.

et al., 1992), while the proximity of the cross-peaks in each state suggested similar β-sheet structures for the two states. β-Sheet conformation is further indicated by the presence of 8−10 Hz $^3J_{\alpha N}$ coupling constants, low NH temperature factors, and strong sequential αH−NH and long-range αH−αH NOEs (among many others). A portion of the αH−αH region from a NOESY spectrum is shown in Figure 1B. Approximately eight αH−αH cross-peaks are apparent. M9−V22 and L11−I20 αH−αH cross-peaks (boxed-in), which establish the sequence alignment for β-sheet strands 1 and 2, are clearly duplicated, indicating the same sheet alignment in either conformational state. V7−L24 αH−αH NOE cross-peaks are observed under different conditions. The alignment of strands 2 and 3 can be deduced from the I21−S31 αH−αH cross-peak (Figure 1B). A potential K23−E29 αH−αH NOE could not be observed due to resonance overlap; however, other NOEs confirm their alignment. Although the I21−S31 αH−αH NOE cross-peak appears not to be duplicated due to chemical shift degeneracy of resonances in both states, its intensity is nearly double that of those showing duplicates. The best explanation for this is that the conformation at this backbone β-sheet position is essentially the same in each state.

Figure 2 shows a schematic for the folding of βpep-4 based on the observation of numerous interstrand NOEs. Interstrand backbone to backbone NOEs are indicated by arrows. In addition, many cross-strand backbone to side chain and side chain to side chain NOEs were observed. β-Strand alignments depicted in Figure 2 are the same in both conformational states 1 and 2. As mentioned above, βpep-4 was designed (Mayo et al., 1996) to fold as a β-sheet like that found in α-chemokines (Zhang et al., 1994; Mayo et al., 1995; Clore et al., 1990a,b; Baldwin et al., 1991; Mayo et al., 1994; Fairbrother et al., 1994). In fact, βpep-4 strands 2 and 3, proposed to be a folding initiation sequence (Ilyina et al., 1994), are aligned the same as in α-chemokines. On the other hand, the anticipated alignment of strands 1 and 2 is shifted by four residues in βpep-4, resulting in a comparatively shorter β-sheet and first turn/loop. One possible explanation for this is that the α-chemokine N-terminus (21 residues longer in PF4 than in βpep-4), which is covalently linked to the first sheet turn/loop via a cystine disulfide bridge between residues 10 and 36 (residue 15 in βpep-4), forces formation of a different turn/loop structure and longer β-sheet. In support of this, it was observed that when the constraining disulfide bonds are reduced in PF4,

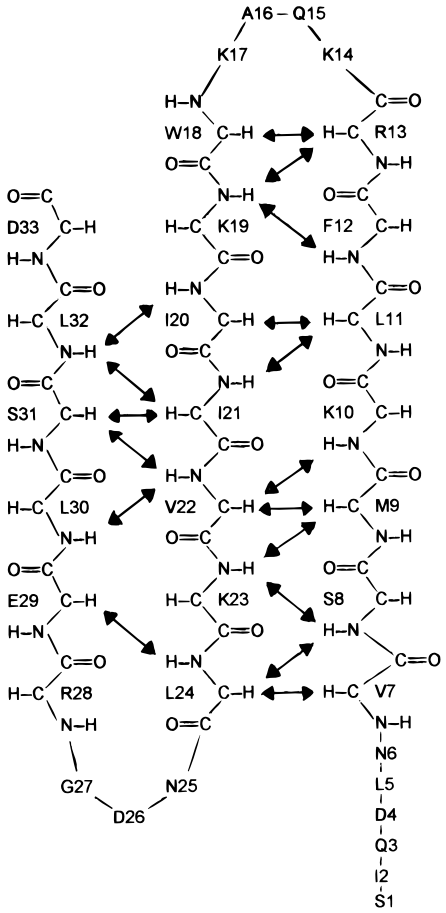

FIGURE 2: β-Strand alignments in βpep-4 monomers. Intramonomer β-sheet residue alignments are shown schematically. Observed backbone−backbone interstrand NOEs are indicated by arrows.

for example, the tetramer dissociates and random coil monomers are only able to form molten globule-like dimers (Mayo et al., 1992), i.e., compact structure is lost.

Continuing with the structural analysis of βpep-4, some NOEs can only be explained by considering inter-monomer (dimer) β-sheet interactions between two strands 1. This was not unexpected since this type of dimer formation is observed in α-chemokines. In conformational state 1, for example, N6−K10 and D4−F12 αH−αH NOEs are evident (Figure 1), as are D4−F12 and F12−D4 βH−αH NOEs (Figure 3), whereas in conformational state 2, these NOEs are not observed while S8−K10 αH−αH (observed under

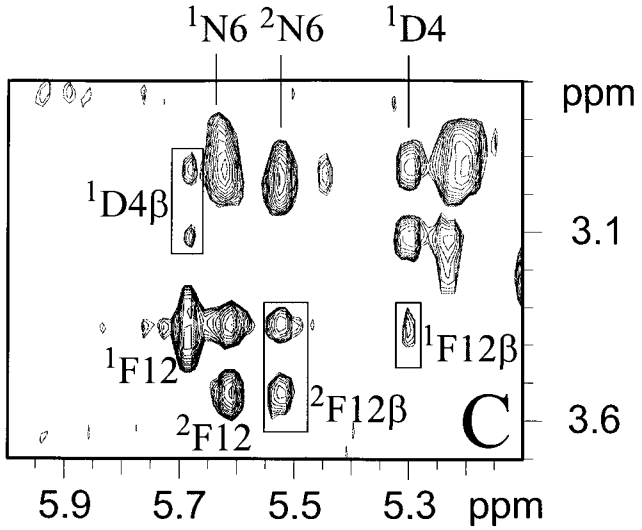

FIGURE 3: NOESY spectrum of βpep-4. An $\alpha H-\beta H_2$ resonance region from a NOESY contour plot is shown for βpep-4 peptide (20 mg/mL) in 20 mM potassium phosphate, pH 6.3, 40 °C. Data were collected in ^2H_2O (99.99%) and acquired/processed as described in the legend to Figure 1. Labeling of resonances is as discussed in the text. Boxed-in cross-peaks denote inter-monomer NOEs which establish strand alignments in the two conformational states. Superscripts 1 and 2 denote conformational states 1 and 2, respectively.

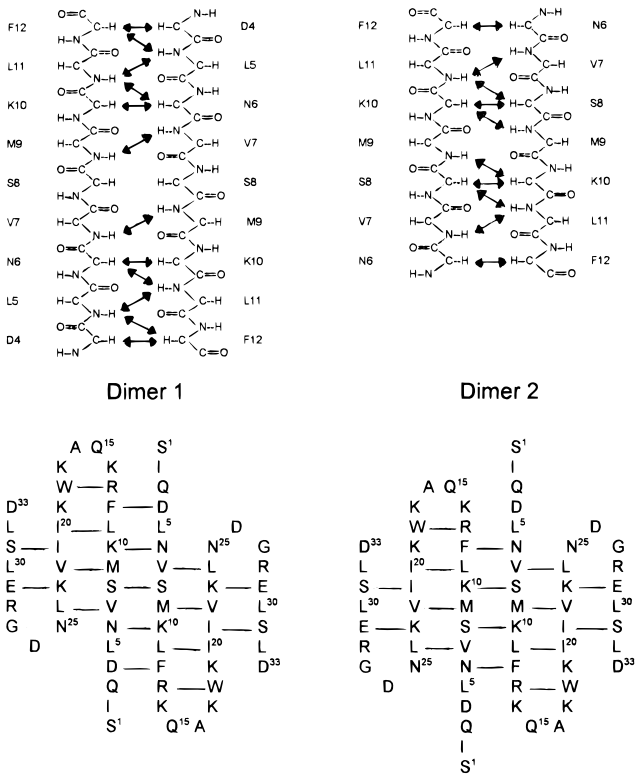

FIGURE 4: Alignment of monomer subunits in dimers 1 and 2. The general alignment of monomers is shown for dimer 1 and dimer 2 at the bottom of the figure. Lines indicate intra- and inter-monomer $\alpha H-\alpha H$ alignments. At the top of the figure, observed inter-monomer backbone−backbone NOEs are indicated by arrows.

different conditions) and F12−N6 $\beta H-\alpha H$ NOEs (Figure 3), for example, are observed. These two distinct patterns of NOEs indicate that conformational duplication arises primarily from a two-residue shift in the interfacial strand 1−strand 1 alignments giving rise to two dimer folds labeled dimer 1 (state 1) and dimer 2 (state 2) in Figure 4 (bottom). Inter-monomer backbone−backbone NOEs observed in dimers 1 and 2 are indicated by arrows in Figure 4 (top). In both states, therefore, dimers are formed by extending their antiparallel β-sheets via interactions between strand 1 from two monomers. These structures help to explain the observation that chemical shifts of resonances from conformational state 1 and state 2 differ most for the sequence D4 to R13 (strand 1), less for W18 to L24 (strand 2), and least for E29 to D33 (strand 3). Chemical shift differences for backbone NH and αH resonances of these residues are listed in Table 1. The average shift difference is 0.09 ppm for ΔNH and 0.1 ppm for ΔαH in strand 1, about half those values in strand 2, and near zero in strand 3. Notice also that these differences are greatest for D4 and L5 whose positions inside and outside of the sheet change the most. A further contribution to D4 chemical shift differences is that, in dimer 1, D4 is in a more hydrophobic environment across from F12 of an opposing strand, whereas in dimer 2 it is positioned across from a lysine, K14.

Table 1: Chemical Shift Differences (in ppm) of NH and αH Resonances, i.e., ΔNH and ΔαH, in βpep-4 β-Sheet Strands 1, 2, and 3[a]

ΔNH, ΔαH		ΔNH, ΔαH		ΔNH, ΔαH	
strand 3		strand 2		strand 1	
		W18	0.05, 0.14	R13	0.05, 0.12
D33	0, 0	K19	0.02, 0.02	F12	0.04, 0.08
L32	0, 0	I20	0.07, 0.07	L11	0.1, 0.09
S31	0, 0	I21	0, 0	K10	0.14, 0.0
L30	0, 0	V22	0.07, 0.01	M9	0.12, 0.07
E29	0.02, 0.07	K23	0.03, 0.02	S8	0.05, 0.06
		L24	0.09, 0.06	V7	0.07, 0.01
				N6	0.04, 0.11
				L5	0.14, 0.03
				D4	0.11, 0.41

[a] Columns represent the individual strands, and rows align residues as shown in the monomer fold in Figures 2 and 4.

For either dimer, the six-stranded β-sheet fold is similar to that observed in α-chemokines (Zhang et al., 1994; Mayo et al., 1995; Clore et al., 1990a,b; Baldwin et al., 1991; Mayo et al., 1994; Fairbrother et al., 1994) from which βpep-4 was designed. For insight into additional details of βpep-4 dimer conformations, structures for dimers 1 and 2 were calculated using NOEs, dihedral angles, and H-bond constraints. Structural calculations were accomplished using a simulated annealing protocol (Brunger, 1992). A total of 280 nonredundant, intra-monomer NOE distance constraints were derived from analysis of NOESY spectra. These include 86 intraresidue, 75 sequential, 46 medium-range ($|i - j| < 5$), and 73 long-range ($|i - j| \geq 5$) constraints. In addition, torsion angle constraints were obtained for 13 ϕ angles. A total of 8 intra-monomer hydrogen bonds could be identified by inspection of initial structures, giving rise to 16 hydrogen bond distance constraints. These hydrogen bond constraints account for the lowest NH temperature factors. The total number of experimentally derived constraints was therefore 309, giving a total of 9.4 constraints per residue. For dimers 1 and 2, 44 and 24 inter-monomer constraints (36 and 14 NOE and 8 and 10 hydrogen bond), respectively, were identified. Addition of these constraints increased the average number of constraints per residue to about 11. All long-range NOEs originated from β-sheet sequences: D4−R13, W18−K23, E29−L32. The average number of constraints arising only from these β-sheet residues is 18.6. Few NOEs were identified in loop/turns K14−K17 and L24−R28 or in the N-terminal segment S1−Q3.

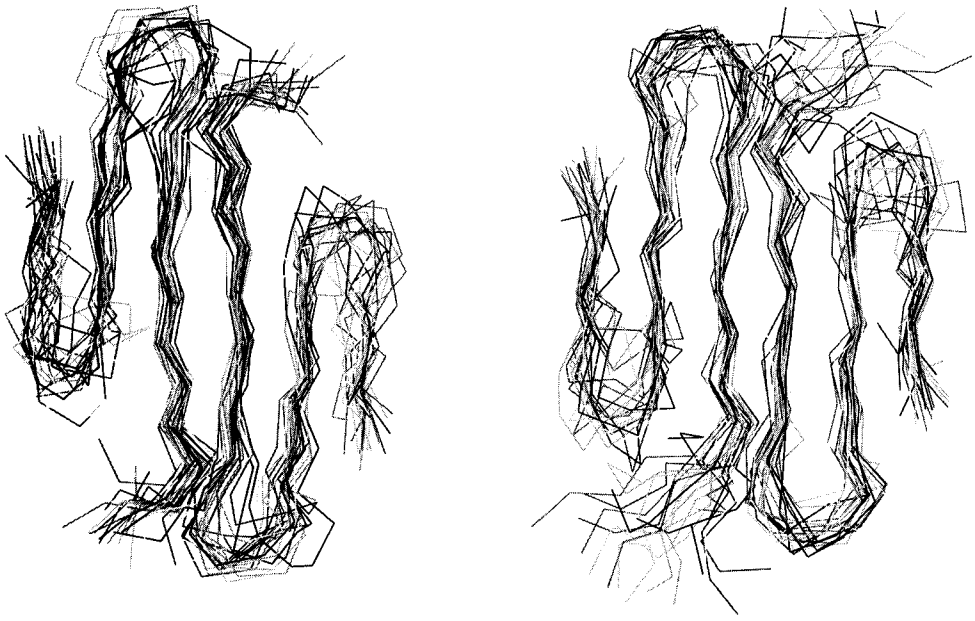

FIGURE 5: Calculated structures for βpep-4 dimers. Twenty-five structures for dimer 1 and dimer 2, calculated by using dynamical simulated annealing, have been superimposed using C_α atoms within the β-sheet.

Table 2: Structural Statistics[a]

	dimer 1	dimer 2
deviations from idealized geometry		
bonds (Å)	0.003	0.003
angles (deg)	0.72 ± 0.04	0.76 ± 0.04
impropers (deg)	0.68 ± 0.05	0.7 ± 0.04
energies (kcal·mol^{-1}) (per dimer)		
E_{NOE}[b]	56 ± 3	62 ± 4
E_{NCS}	25 ± 3	31 ± 4
E_{BOND}	13 ± 1	15 ± 1
E_{ANGLE}	33 ± 2	37 ± 3
$E_{IMPROPER}$	6 ± 1	6 ± 1
E_{TOTAL}	133 ± 14	151 ± 16

[a] The 25 final structures exhibited 7−10 distance restraint violations greater than 0.5 Å and no dihedral angle violations greater than 10°. [b] The final values of the NOE (E_{NOE}) and NCS (E_{NCS}) potentials have been calculated with force constants of 25 kcal·mol^{-1}·Å^{-2} and 300 kcal·mol^{-1}·Å^{-2}, respectively.

For each βpep-4 dimer, 100 structures were calculated, and the 25 best-fit structures have been superimposed (backbone C_α trace) in Figure 5. Structural statistics for these final structures are summarized in Table 2. All satisfy experimental constraints very well. No bad nonbonded contacts were found. For the three β-sheet strands (D4−R13, W18−K23, and E29−L32), average atomic RMS differences with respect to the mean coordinate positions are 0.54 Å (dimer 1) and 0.63 Å (dimer 2) for backbone (N, C_α, C) atoms and 1.35 Å (dimer 1) and 1.57 Å (dimer 2) for all heavy atoms. In addition, ϕ and ψ angular order parameters are all >0.8 for either dimer, indicating relatively well-defined backbone dihedral angles (Hyberts et al., 1992). For loop/turn backbone atoms, average RMSD values range from 1.6 to 6 Å (N-terminus). The backbone torsion angles for non-glycine residues lie within allowed Ramachandran ϕ,ψ space. Together, the above data indicate that all structures used to represent the solution structures of both βpep-4 dimers are well converged. Both dimers show characteristic right-handed twists in their six-stranded β-sheets. The β-sheet twist in dimer 1 is slightly greater than it is in dimer 2, possibly the result of a longer inter-monomer sheet in dimer 1. In either dimer, however, the surface of the sheet is amphipathic with the central residues on the hydrophobic side consisting of V7, M9, L11, W18, I20, V22, L24, L30, and L32.

Pulse field gradient NMR diffusion measurements have established that βpep-4 forms tetramers in solution (Mayo et al., 1996) with no evidence for free monomers and about 5% dimers at 5 mM peptide (unpublished results). In fact, even at 0.04 mM, βpep-4 remains at about 30% tetramer. Under the conditions of these NMR experiments, therefore, it may be concluded that 90% to 95% dimers exist only within tetramers. This being the case, these amphipathic dimers most probably associate to form a β-sheet sandwich with their hydrophobic surfaces at the interface. Hydrophobically-mediated dimer−dimer association is supported by the temperature dependence of βpep-4 self-association (Tanford, 1981) which increases as the temperature is increased from 5 to 40 °C (Mayo et al., 1996). In this β-sheet sandwich, the sequences V7 to F12 and I20 to K23 from each subunit would be at the core of the tetramer. This is consistent with the observation that backbone NHs of S8, M9, K10, and I21 show the lowest NH temperature factors (0.02−0.03 ppb K^{-1}) (Kim et al., 1993), followed by V7, L11, F12, R13, K19, I20, V22, and L30 (0.04−0.05 ppb K^{-1}).

The next question to be addressed is whether βpep-4 dimers associate as two different homotetramers and/or as one heterotetramer composed of dimers 1 and 2. The type of βpep-4 tetramer cannot be differentiated from pulsed field gradient NMR self-association measurements (Mayo et al., 1996). Since TOCSY cross-peak intensities of dimers 1 and 2 are equal, it is perhaps more likely that heterotetramers are formed since, from a thermodynamic perspective, it is less likely that these two different homotetramers would be equally populated. Considering dimer interactions alone, dimer 1 can form eight intersubunit hydrogen bonds and four intersubunit hydrophobic residue pairings, whereas dimer 2 can form only six intersubunit hydrogen bonds and three

intersubunit hydrophobic residue pairings. In a homotetramer, dimer 2−dimer 2 interactions would have to compenstate for these differences in order to achieve thermodynamic equality with a dimer 1−dimer 1 homotetramer. Clearly, however, the best evidence for the existence of heterotetramers would be the observation of NOEs between residues from dimer 1 and dimer 2; however, identification of potential inter-dimer NOEs is hindered by overlap of resonances from interfacial dimer residues which are primarily aliphatic. The only interfacial aromatic residue is W18, and overlap of W18 and F33 aromatic resonances also makes identification of potential NOEs between W18 and aliphatic side chain resonances ambiguous. Interestingly, native PF4 is a tetramer of homodimers which associate asymmetrically (Zhang et al., 1994; Mayo et al., 1995). PF4 heterodimers do not form primarily due to conformationally stabilizing inter-monomer interactions between the sheet and a C-terminal helix which is absent in βpep-4.

Regardless of the type of βpep-4 tetramer formed, an additional structural feature in the β-sheet sandwich is its highly positively charged surface, i.e., net positive charge of +20. This makes βpep-4 and other βpep peptides (Mayo et al., 1996) good candidates for binding to anionic biomolecules like heparin and cell surface heparan sulfate and possibly for modulating various cellular activities. PF4 and other α-chemokines on which the βpep design was based also have a relatively high net positive surface charge, bind polysulfated glycosaminoglycans like heparin, and trigger various cellular activities (Miller & Krangel, 1992). βpep-4 and related homologs may be novel chemokines, and it would be interesting to investigate potential chemokine-like biological activities.

ACKNOWLEDGMENT

NMR experiments were performed at the University of Minnesota High Field NMR Laboratory. Peptides were synthesized at the Microchemical Facility, Institute of Human Genetics, University of Minnesota. We are grateful to Dinesha S. Walek for her expertise in peptide synthesis.

SUPPORTING INFORMATION AVAILABLE

Supporting information for this paper consists of one table giving ^{1}H NMR chemical shifts for the peptide, βpep-4 (5 pages). Ordering information is given on any current masthead page.

REFERENCES

Baldwin, E. T., Weber, I. T., St. Charles, R., Xuan, J.-C., Appella, E., Yamada, M., Matsushima, K., Edwards, B. F. P., Clore, G. M., Gronenborn, A. M., & Wlodawer, A. (1991) *Proc. Natl. Acad. Sci. U.S.A. 88*, 502−506.

Bax, A., & Davis, D. G. (1985) *J. Magn. Reson. 65*, 355−360.

Blanco, F. J., Rivas, G., & Serrano, L. (1994) *Struct. Biol. 1*, 584−590.

Brunger, A. (1992) *Xplor (Version 3.1) Manual*, Yale University Press, New Haven, CT.

Bryson, J. W., Betz, S. F., Lu, H. S., Suich, D. J., Zhou, H. X., O'Neil, K. T., & DeGrado, W. F. (1995) *Science 270*, 935−941.

Clore, G. M., Appella, E., Yamada, M., Matsushima, K., & Gronenborn, A. M. (1990a) *Biochemistry 29*, 1689−1696.

Clore, G. M., Bax, A., Wingfield, P. T., & Gronenborn, A. M. (1990b) *Biochemistry 29*, 5671−5676.

DeGrado, W., Wasserman, Z., & Lear J. (1989) *Science 243*, 622−628 .

Fairbrother, W. J., Reilly, D., Colby, T. J., Hesselgesser, J., & Horuk, R. (1994) *J. Mol. Biol. 242*, 252−270.

Fedorov, A. N., Dolgikh, D. A., Chemeris, V. V., Chernov, B. K., Finkelstein, A. V., Schulga, A. A., Alakhov, Y. B., Kirpichnikov, M. P., & Ptitsyn, O. B. (1992) *J. Mol. Biol. 223*, 927−931.

Fezoui, J., Weaver, D. L., Osterhout, J. J. (1994) *Proc. Natl. Acad. Sci. U.S.A. 91*, 3675−3679.

Hahn, K., Klis, W., & Stewart, J. (1990) *Science 248*, 1544−1547.

Handel, T. M., Williams, S. A., & DeGrado, W. F. (1993) *Science 261*, 879−885.

Hecht, M., Richardson, J., Richardson, D., & Ogden, R. (1990) *Science 249*, 884−891.

Hyberts, S., Goldberg, M. S., Havel, T. F., & Wagner, G. (1992) *Protein Sci. 1*, 736.

Ilyina, E., & Mayo, K. H. (1995) *Biochem. J. 306*, 407−419.

Ilyina, E., Milius, R., & Mayo, K. H. (1994) *Biochemistry 33*, 13436−13444.

Jeener, J., Meier, B., Backman, P., & Ernst, R. R. (1979) *J. Chem. Phys. 71*, 4546−4550.

Kamteker, S., Schiffer, J. M., Xiong, H., Babik, J. M., & Hecht, M. H. (1993) *Science 262*, 1680−1685.

Kim, C. A., & Berg, J. M. (1993) *Nature 362*, 267−270.

Kim, K.-S., Fuchs, J. A., & Woodward, C. K. (1993) *Biochemistry 32*, 9600−9608.

Kuroda, Y., Nakai, T., & Ohkubo, T. (1994) *J. Mol. Biol. 236*, 862−868.

Marion, D., & Wüthrich, K. (1983) *Biochem. Biophys. Res. Commun. 113*, 967−975.

Marion, D., Ikura, M., Tschudin, R., & Bax, A. (1985) *J. Magn. Reson. 89*, 393−399.

Mayo, K. H., Barker, S., Kuranda, M. J., Hunt, A. J., Myers, J. A., & Maione, T. E. (1992) *Biochemistry 31*, 12255−12265.

Mayo, K. H., Yang, Y., Daly, T. J., Barry, J. K., & La Rosa, G. J. (1994) *Biochem. J. 304*, 371−376 .

Mayo, K. H., Roongta, V., Ilyina, E., Milius, R., Barker, S., Quinlan, C., La Rosa, G., & Daly, T. J. (1995) *Biochemistry 34*, 11399−11409.

Mayo, K. H., Ilyina, E., & Park, H. (1996) *Protein Science 5*, 1301−1315.

Miller, M. D., & Krangel, M. S. (1992) *Crit. Rev. Immunol. 12*, 17−46.

Minor, D. L., Jr,, & Kim, P. S. (1994) *Nature 367*, 660−663.

Minor, D. L., Jr., & Kim, P. S. (1994) *Nature 371*, 264−267.

Nilges, M. *Proteins: Struct., Funct., Genet. 17*, 297−308 (1993).

Otzen, D. E., & Fersht, A. R. (1995) *Biochemistry 34*, 5718−5724.

Piantini, U., Sørensen, O. W., & Ernst, R. R. (1982) *J. Am. Chem. Soc. 104*, 6800−6801.

Quinn, T. P., Tweedy, N. B., Williams, R. W., Richardson, J. S., & Richardson, D. C. (1994) *Proc. Natl. Acad. Sci. U.S.A. 91*, 8747−8751.

Regan, L., & DeGrado, W. (1988) *Science 241*, 976−978.

Richardson, J. S., Richardson, D. C., Tweedy, N. B., Gernert, K. M., Quinn, T. P., Hecht, M. H., Erickson, B. W., Yang, Y., McClain, R. D., Donlan, M. E., & Surles, M. C. (1992) *Biophys. J. 63*, 1185−1209.

Searle, M. S., Williams, D. H., & Packman, L. C. (1995) *Nature, Struct. Biol. 2*, 999−1006.

Shaka, A. J., & Freeman, R. (1983) *J. Magn. Reson. 51*, 169−173.

Smith, C. K., Withka, J. M., & Regan, L. (1994) *Biochemistry 33*, 5510−5517.

States, D. J., Haberkorn, R. A., & Ruben, D. J. (1982) *J. Magn. Reson. 48*, 286−293.

Stewart, J. M., & Young, J. D. (1984) *Solid Phase Peptide Synthesis*, 2nd ed., pp 135, Pierce Chemical Co., Rockford, IL.

Struthers, M. D., Cheng, R. P., & Imperiali, B. (1996) *Science 271*, 342−345.

Tanford, C. (1981) *Physical Chemistry of Macromolecules*, pp 286−296, Wiley, New York.

Wider, G., Macura, S., Anil-Kumar, Ernst, R. R., & Wüthrich, K. (1984) *J. Magn. Reson. 56*, 207−234.

Wishart, D. S., Sykes, B. D., & Richards, F. M. (1992) *Biochemistry 31*, 1647−1651.

Yan, Y., & Erickson, B. W. (1994) *Protein Sci. 3*, 1069−1073.

Zhang, X., Chen, L., & Bancroft, D. P. (1994) *Biochemistry 33*, 8361−8366.

BI963064O